Dalton Transactions

ROYAL SOCIETY OF CHEMISTRY

COMMUNICATION

View Article Online
View Journal | View Issue

Check for updates

Cite this: *Dalton Trans.*, 2024, **53**, 16821

Received 20th September 2024,
Accepted 30th September 2024

DOI: 10.1039/d4dt02670e

rsc.li/dalton

Water stable colloidal PVP coated spin crossover nanoparticles†

Christina D. Polyzou, *[a] Eleni Zygouri, [a] Nikolia Lalioti, [a] Ondrej Malina, *[b,c] Michaela Polaskova,[b] Jiri Bednar[c] and Vassilis Tangoulis *[a]

Stable aqueous dispersions of spin-crossover (SCO) doped $[Fe^{II}(Htrz)_2(trz)](BF_4)$ nanoparticles (NPs) were prepared by using water-soluble polyvinylpyrrolidone (PVP) as protecting polymer. The metal or ligand substitution percentage regulated the ultra-small size and morphology of the NPs. At the same time, the colloidal dispersions showed a complete conversion of the LS state to the HS state of the Fe^{II} ion.

In the last decade, nanosized spin crossover (SCO) materials have been in the foreground as their miniaturization is promising for potential technological and medical applications. Molecular switches, memory storage devices, and photonic/electronic/mechanical devices compose one side of the coin,[1–9] while drug delivery, cancer therapy, and MRI bioimaging are the second one.[10–18] However, in all cases, the preservation of spin transition cooperativity close to room temperature during the downsizing of the compounds in the nanoscale and the size control are considered of utmost importance. For this reason, the scientific interest has been recently focused on one-dimensional (1D) SCO Fe–triazole coordination polymers of the type $[Fe^{II}(4R\text{-}1,2,4\text{-}Trz)_3]X_2{\cdot}nH_2O$ (R = H, NH_2, X = BF_4^-, ClO_4^-) and on their metal and ligand substituted derivatives.[19–27] The latter ones are considered "doped" nanoparticles (NPs) with improved magnetic properties in the frames of narrower hysteresis centred closer to room temperature.

One of the leading synthetic protocols used mainly for synthesizing doped NPs is the reverse micelle method, which results in a rule in well-shaped and size-controlled NPs. In 2007, Coronado *et al.*[19] reported for the first time $[Fe(Htrz)_2(trz)](BF_4)$ NPs with the smallest so far size of 10 nm and the SCO doped $[Fe_{0.8}Zn_{0.2}(Htrz)_2(trz)](BF_4)$ NPs using the same synthetic approach leading to a shifted hysteresis loop closer to room temperature. In 2019, Bello *et al.*[26] reported a series of SCO doped $[Fe(Htrz)_{1+y-x}(trz)_{2-y}(NH_2trz)_x](BF_4)_y$ NPs with the precipitation method. Their spin-transition shifted progressively toward room temperature with increasing the percentage of 4-NH_2-triazole, parallel with a decrease in hysteresis width and abruptness. A drawback of this method was the absence of any surfactant or polymer in the synthetic procedure, which led to inhomogeneity and aggregation of the doped NPs.

During the efforts to stabilize aqueous dispersions of the doped NPs -an essential property for biological applications- our research group recently reported a series of silicon-based SCO doped $[Fe_z/Zn_{1-z}(Htrz)_{1+y-x}(trz)_{2-y}(NH_2trz)_x](BF_4)_y$ NPs[28] synthesized through the reverse micelle method, preserving all the desired spin transition characteristics and stabilized aqueous dispersions which make these promising for MRI applications. Following a reverse micelle protocol, another family of silica-based Fe/triazole NPs of the type $[Fe(NH_2trz)_3](NO_3)_2@SiO_2$ has been recently reported to remain stable in water for up to two hours, revealing a water-induced spin transition.[29] In light of these findings, we have embarked on the challenge of developing facile, surfactant-free, and one-pot syntheses of SCO NPs focusing on preserving the SCO characteristics in aqueous dispersions for a long period of time and avoiding time-consuming reverse micelle procedures accompanied by several cleaning cycles of surfactant residues.[28,29]

Herein, we present the synthesis of highly dispersed doped surfactant-free NPs based on the already known 1D SCO coordination polymer $[Fe^{II}(Htrz)_2(trz)](BF_4)$ controlled by poly (vinylpyrrolidone) (PVP) as a protecting polymer.[30,31] It is also essential to notice that in the aqueous dispersions of PVP-supported doped NPs, the evolution of the SCO phenomenon

[a]*Department of Chemistry, Laboratory of Inorganic Chemistry, University of Patras, 26504 Patras, Greece. E-mail: chpolyzou@upatras.gr, vtango@upatras.gr*
[b]*Regional Centre of Advanced Technologies and Materials, Czech Advanced Technology and Research Institute (CATRIN), Palacký University Olomouc, Křížkovského 511/8, 77900, Czech Republic. E-mail: ondrej.malina@upol.cz*
[c]*CEET, Nanotechnology Centre, VŠB–Technical University of Ostrava, 17. listopadu 2172/15, Ostrava, Poruba 708 00, Czech Republic. E-mail: ondrej.malina@vsb.cz*

†Electronic supplementary information (ESI) available: Experimental details, IR spectra, pXRD data, TEM images, DSC measurements, UV-Vis spectra. See DOI: https://doi.org/10.1039/d4dt02670e

results in the complete conversion of the LS state to the HS state of the Fe^{II} ion. In the literature, PVP is well-known for preventing aggregation of NPs,[32] while its solubility in water makes it promising for biomedical and pharmaceutical applications.[32–34] This is also due to its biocompatibility and potential to stabilize aqueous dispersions of protected NPs.[35] PVP was chosen as the macromolecule polymer substrate due to its solubility, film-forming properties, environmental friendliness, and ability to form hydrogen bonds with compounds. A composite film $[Fe(NH_2trz)_3(ClO_4)_2]$-PVP was synthesized from a solution of PVP, NH_2trz, and $Fe(ClO_4)_2$ in ethanol to create a homogeneous film with a regular nano-scale structure exhibiting regular striped patterns in the nano-scale, indicating a crystalline structure different from typical amorphous solid compounds.[36] PVP-coated nanoparticles of $[Fe(hptrz)_3](OTs)_2$ (hptrz = 4-heptyl-1,2,4-triazole, Ts = *para*-toluenesulfonyl) were synthesized in homogeneous media by preparing solutions with specific components, leading to nanoparticle precipitation and the formation of 200–400 nm crystals of the spin-crossover complex.[37]

The general formula of the synthesized NPs is $[Fe(Htrz)_2(trz)](BF_4)$@1.4PVP (**NP1**); for the metal substituted NPs: $[Fe_{0.8}Zn_{0.2}(Htrz)_2(trz)](BF_4)$@1.3PVP (**NP2**); for the ligand substituted NPs: $[Fe(Htrz)_2(trz)_{0.7}(NH_2trz)_{0.3}](BF4)_{1.3}$@0.6PVP (**NP3**). All the NPs were synthesized at room temperature using an *ex situ* synthetic method.[38] The aim is to investigate the influence of the metal/ligand substitution on the size, shape, and spin transition properties of these nanoparticles and the effect of the PVP on the homogeneity of the NPs and their stabilization of aqueous dispersions. Their physical and structural characterization was carried out by FT-IR and UV-Vis (UV-Vis) spectroscopy, Elemental Analysis (EA), and powder X-ray diffraction (p-XRD). The SCO behavior was determined using magnetic and differential scanning calorimetry (DSC) studies, while the size, morphology, and distribution of the NPs were determined with Transmittance Electronic Spectroscopy (TEM) and Dynamic light scattering (DLS).

NP1 was prepared by an *ex situ* reaction method mixing a suspension of $Fe(BF_4)_2{\cdot}6H_2O$ and PVP in EtOH with a solution of Trz and PVP in EtOH. The metal/ligand molecular ratio was 1 : 3. **NP2** and **NP3** were synthesized using an analogous experimental procedure by partial replacement of $Fe(BF_4)_2{\cdot}6H_2O$ and the deprotonated trz ligand by $Zn(BF_4)_2{\cdot}6H_2O$ and the NH_2trz ligand, respectively. In particular, partial replacement of 20% of the $Fe(BF_4)_2{\cdot}6H_2O$ by the Zn^{II} analog resulted in doped **NP2**. In comparison, partial replacement of 30% of the deprotonated trz ligand by the NH_2trz derivative resulted in doped **NP3**. The molar ratios of Fe^{II}/Zn^{II}/Trz and Fe^{II}/Trz/NH_2trz reagents used for their syntheses were 0.8 : 0.2 : 1 and 1 : 2.7 : 0.3, respectively (the percentage of the Zn dopant ion was confirmed by EDS analysis shown in Fig. S1†). In all cases, the **NP1**, **NP2**, and **NP3** were coated with the same quantity of PVP, forming well-shaped spherical nanoparticles. P-XRD and EA were used to support the identity and purity of all compounds (Fig. 1, Fig. S1 and Table S1†). The IR spectra of all NPs showed very strong stretch vibrational modes at around 1650 cm^{-1}, which can be attributed to the presence of the C=O group of PVP (Fig. S2†). According to the reported magnetic properties of the 1D coordination polymer $[Fe^{II}(Htrz)_2(trz)](BF_4)$, two different polymorphs (**I** and **II**) have been identified[39] which are crystallized in the same space group, *Pnma*. Polymorph **I** with lattice parameters (a, b, c, V) = (17.294(6) Å, 7.337(2) Å, 9.182(3) Å, 1165.1(6) $Å^3$) reveals a large hysteresis of 40 K centered at 370 K while a smaller one of 15 K is centered at 330 K and corresponds to polymorph **II** where the lattice parameters are: (a, b, c, V) = (16.691(6) Å, 7.338(2) Å, 9.482(3) Å, 1161.3(5) $Å^3$). The Le–Bail method was used to calculate the lattice parameters of the **NP1–3**, and the obtained values are shown in Table S2.† According to the diffraction pattern profiles of **NP1–3** (Fig. 1), where a single peak appears at around 10.6° in 2θ values denoting the proximity of 101 and 200 *hkl* reflections, all final products are characterized as polymorphs **II**. The TEM images and size distributions of the **NP1–3** are presented in Fig. 1 and S3,† and the calculated mean diameter of sphere-like NPs is 30 nm, 20 nm, and 10 nm, respectively.

Temperature-dependent magnetic and DSC measurements were carried out on **NP1–3**, and the third thermal cycle is shown in Fig. 1. Upon cooling, abrupt thermal hysteresis occurs for **NP1**. At 300 K, the value of the $\chi_M T$ product equals 3.0 emu K mol^{-1} for all NPs, which is typical for Fe^{II} in the high-spin (HS) state. The hysteresis appears at critical temperatures $T_c\downarrow$ = 323 K and $T_c\uparrow$ = 355 K for **1** with width of *ca.* 32 K. However, doped **NP2** and **NP3**, where metal and ligand substitutions occur, shift the hysteresis clearly toward room temperature with loss of its abruptness and narrowing of its width. The critical temperatures are $T_c\downarrow$ = 294 K, $T_c\uparrow$ = 309 K for **NP2** and $T_c\downarrow$ = 299 K, $T_c\uparrow$ = 314 K for **NP3**, respectively, with hysteresis loop widths both of *ca.* 15 K. The SCO behavior exhibited by all the NPs was also confirmed through DSC measurements (Fig. 1, S4 and Table S3†).

UV-vis measurements were carried out to verify the reversibility of the SCO phenomenon in water following a protocol described in Fig. S4.† According to this protocol, SCO NPs synthesized without PVP coating revealed sedimentation issues, accompanied by discoloration of the solution, verifying the oxidation of the Fe(II) ions (Fig. S5†). Fig. S6† shows the UV-vis absorption spectra of **NP1–3** when the samples are dispersed for the first time in H_2O, while Fig. 2 presents the temperature dependence of the UV-vis spectra during the thawing procedure (−20 °C to RT). In both cases, the absorption band around 280 nm -corresponding to an MLCT transition-showed a drastic reduction of its intensity as the samples switched from the LS to the HS state of Fe^{II}, accompanied by a color change in the dispersion from purple to yellow (Fig. 2, Fig. S4 and Fig. S6†). The mechanism of spin crossover in water for Fe(II) complexes with triazoles[40] involves several critical factors, such as: (a) Hydration effects according to which water molecules interact with the metal centre of the complexes, influencing the coordination environment and altering the energy levels of the metal d-orbitals. This interaction can stabilize or destabilize specific spin states, impacting the equilibrium

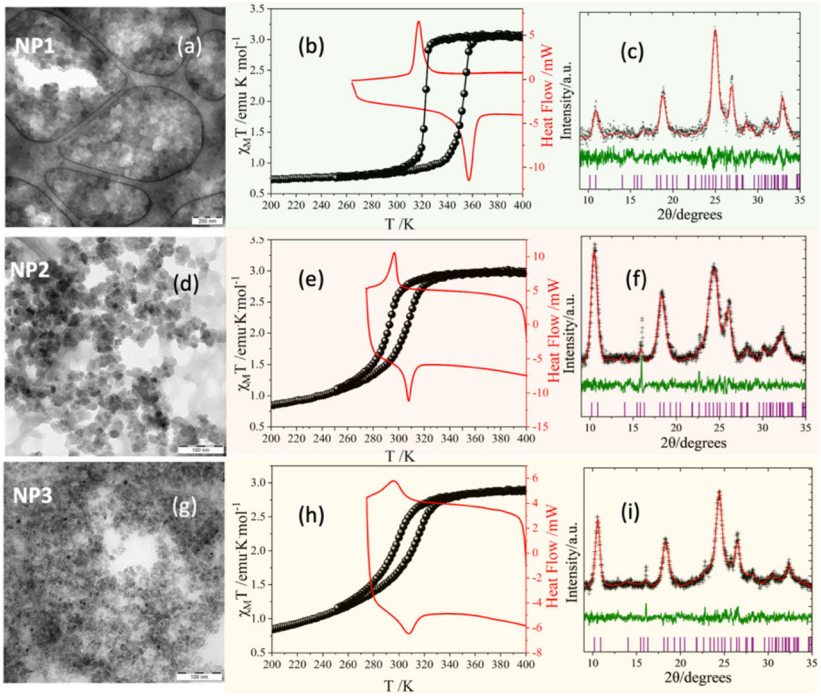

Fig. 1 TEM images of (a) **NP1** (scale bar 200 nm), (d) **NP2** (scale bar 100 nm) and (g) **NP3** (scale bar 100 nm); third thermal cycle of the magnetic susceptibility $\chi_M T(T)$ (black spheres) and DSC curve (red line) at 10 K min^{-1} of (b) **NP1**, (e) **NP2** and (h) **NP3** SCO NPs; p-XRD diffraction data (black crosses) and Rietveld refinement using the Le Bail method (red line) of (c) **NP1**, (f) **NP2** and (i) **NP3** SCO NPs. The difference ($I_{calc} - I_{obs}$) is presented as green line, and the theoretical peaks are presented as violet bars.

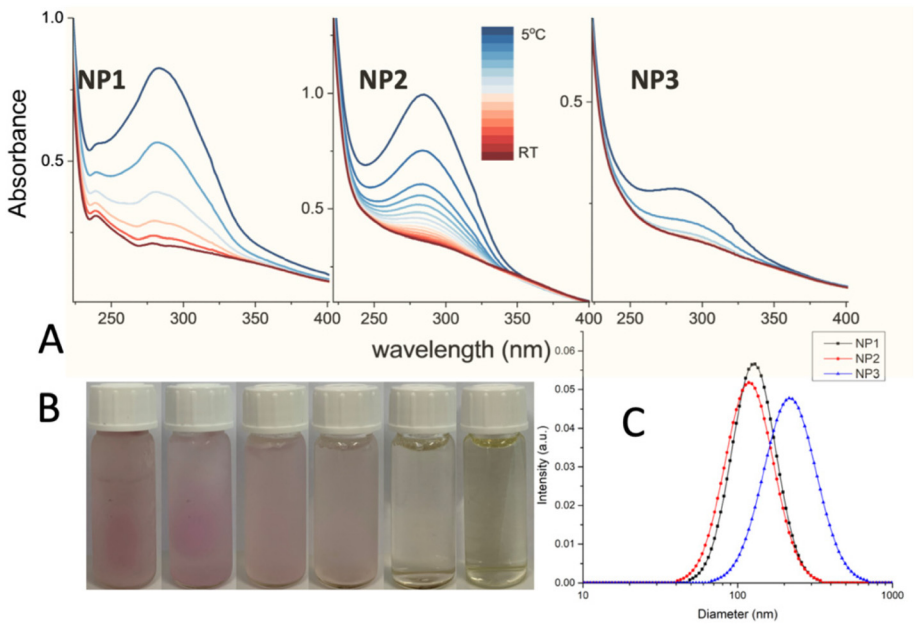

Fig. 2 (A) Temperature dependence of UV-Vis spectra of **NP1–3** in water solution during the thawing procedure. (B) The evolution of the colour in the water dispersion of **NP1–3** during the thawing procedure (from left to right). (C) DLS particle size analysis of **NP1–3**.

between low-spin and high-spin states; (b) Stabilization by hydrogen bonding, according to which the presence of hydrogen bonds between the solvent and the complex leads to a more pronounced stabilization of the low-spin state, affecting the spin crossover behaviour. Quite significantly, freezing and melting processes in aqueous solutions containing Fe(II) complexes can induce structural changes in the complexes, affecting their spin states. It has been found that compression

of polymeric molecules during freezing may lead to transitions into low-spin states, contributing to the observed spin crossover phenomena in solution.[41] Similar phenomena have been described in our previous report where SCO NPs of the same family where synthesized using a reverse micelle method and successfully covered/protected with silica.[28]

DLS measurements (Fig. 2 and Fig. S7†) showed particles agglomerates with *Z*-average 109 nm and PDI 0.11 for **NP1**; *Z*-average 98 nm and PDI 0.14 for **NP2**; *Z*-average 174 nm and PDI 0.16 for **NP3**. Long term size distribution measurements (Fig. S8†) confirmed good stability of samples, which maintained PDI below 0.17 after ~2 days. The control measurement after 7 days showed just slight change in *Z*-average and PDI (see Fig. S9†).

In conclusion, an *ex situ* method is presented for the preparation of PVP-coated doped SCO NPs of the general formula $[FexZn_{1-x}(Htrz)_2(trz)](BF_4)$@PVP and $[Fe(Htrz)_{3-3X}(NH_2trz)_3X](BF_4)$@PVP. The sphere-like NPs adopted sizes close to ultrasmall, with **NP3** between 5 and 10 nm exhibiting SCO hysteretic behavior close to RT. Stable aqueous colloidal dispersions were prepared with apparent reversibility of the SCO phenomenon and complete conversion from LS to HS state accompanied by a color change from purple (LS state) to yellow (HS state) due to the protecting PVP polymer.

Our present communication describes an effective experimental method for preparing downsized PVP-coated doped NPs presenting stable aqueous colloidal dispersions with hysteretic SCO behavior close to RT essential for future drug delivery and MRI-bioimaging perspectives.

Data availability

The data supporting this article have been included as part of the ESI.†

Conflicts of interest

There are no conflicts to declare.

Acknowledgements

O.M., M.P. and J.B. would like to thank to the following projects: the Research Infrastructure NanoEnviCz, supported by the Ministry of Education, Youth and Sports of the Czech Republic under Project No. LM2023066; the project REFRESH – Research Excellence For Region Sustainability and High-tech Industries project number CZ.10.03.01/00/22_003/0000048 *via* the Operational Programme Just Transition; PolyEnvi21 Centre of Competence project No. TN7503813; and project No. CZ.02.01.01/00/22_008/0004631 Materials and technologies for sustainable development within the Jan Amos Komensky Operational Program financed by the European Union and from the state budget of the Czech Republic.

References

1 O. Kahn and C. J. Martinez, *Science*, 1998, **279**, 44–48.
2 O. Kahn, J. Krober and C. Jay, *Adv. Mater.*, 1992, **4**(11), 718–728.
3 A. Bousseksou, G. Molnár, L. Salmon and W. Nicolazzi, *Chem. Soc. Rev.*, 2011, **40**(6), 3313–3335.
4 O. Roubeau, *Chem. – Eur. J.*, 2012, **18**(48), 15230–15244.
5 P. Gutlich, A. Hauser and H. Spiering, *Angew. Chem., Int. Ed. Engl.*, 1994, **33**(20), 2024–2054.
6 *Spin Crossover in Transition Metal Compounds: Topics in Current Chemistry*, ed. P. Gűtlich and H. A. Goodwin, Springer, Berlin, 2004.
7 *Spin Crossover Materials: Properties and Applications*, ed. M. A. Halcrow, John Wiley & Sons Ltd, New York, 2013.
8 G. Molnár, S. Rat, L. Salmon, W. Nicolazzi and A. Bousseksou, *Adv. Mater.*, 2018, **30**, 17003862.
9 K. S. Kumar and M. Ruben, *Coord. Chem. Rev.*, 2017, **346**, 176–205.
10 Y. H. Hu, T. Lv, Y. Ma, J. J. Xu, Y. H. Zhang, Y. L. Hou, Z. J. Huang and Y. Ding, *Nano Lett.*, 2019, **19**(4), 2731–2738.
11 M. Rezaei, A. Abbasi, R. Dinarvand, M. Jeddi-Tehrani and J. Janczak, *ACS Appl. Mater. Interfaces*, 2018, **10**(21), 17594–17604.
12 C. B. He, C. Poon, C. Chan, S. D. Yamada and W. B. Lin, *J. Am. Chem. Soc.*, 2016, **138**(18), 6010–6019.
13 I. Imaz, M. Rubio-Martínez, L. García-Fernández, F. García, D. Ruiz-Molina, J. Hernando, V. Puntes and D. Maspoch, *Chem. Commun.*, 2010, **46**(26), 4737–4739.
14 X. P. Duan, C. Chan, W. B. Han, N. N. Guo, R. R. Weichselbaum and W. B. Lin, *Nat. Commun.*, 2019, **10**, 1899.
15 J. J. Liu, H. R. Wang, X. Yi, Y. Chao, Y. H. Geng, L. G. Xu, K. Yang and Z. Liu, *Adv. Funct. Mater.*, 2017, **27**(44), 1703832.
16 J. J. Liu, L. L. Tian, R. Zhang, Z. L. Dong, H. R. Wang and Z. Liu, *ACS Appl. Mater. Interfaces*, 2018, **10**(50), 43493–43502.
17 S. Suárez-García, N. Arias-Ramos, C. Frias, A. P. Candiota, C. Arús, J. Lorenzo, D. Ruiz-Molina and F. Novio, *ACS Appl. Mater. Interfaces*, 2018, **10**(45), 38819–38832.
18 Y. Chen, K. L. Ai, J. H. Liu, X. Y. Ren, C. H. Jiang and L. H. Lu, *Biomaterials*, 2016, **77**, 198–206.
19 E. Coronado, J. R. Galán-Mascarós, M. Monrabal-Capilla, J. García-Martínez and P. Pardo-Ibáñez, *Adv. Mater.*, 2007, **19**(10), 1359.
20 J. R. Galán-Mascarós, E. Coronado, A. Forment-Aliaga, M. Monrabal-Capilla, E. Pinilla-Cienfuegos and M. Ceolin, *Inorg. Chem.*, 2010, **49**(12), 5706–5714.
21 S. Titos-Padilla, J. M. Herrera, X. W. Chen, J. J. Delgado and E. Colacio, *Angew. Chem., Int. Ed.*, 2011, **50**(14), 3290–3293.
22 M. Giménez-Marqués, M. L. G. S. de Larrea and E. Coronado, *J. Mater. Chem. C*, 2015, **3**(30), 7946–7953.
23 J. M. Herrera, S. Titos-Padilla, S. J. A. Pope, I. Berlanga, F. Zamora, J. J. Delgado, K. V. Kamenev, X. Wang,

A. Prescimone and E. K. Brechin, *J. Mater. Chem. C*, 2015, **3**(30), 7819–7829.
24 I. Suleimanov, J. S. Costa, G. Molnár, L. Salmon and A. Bousseksou, *Chem. Commun.*, 2014, **50**(86), 13015–13018.
25 S. Rat, M. Piedrahita-Bello, L. Salmon, G. Molnár, P. Demont and A. Bousseksou, *Adv. Mater.*, 2018, **30**(8), 1705275.
26 M. Piedrahita-Bello, K. Ridier, M. Mikolasek, G. Molnár, W. Nicolazzi, L. Salmon and A. Bousseksou, *Chem. Commun.*, 2019, **55**(33), 4769–4772.
27 R. Torres-Cavanillas, L. Lima-Moya, F. D. Tichelaar, H. W. Zandbergen, M. Giménez-Marqués and E. Coronado, *Dalton Trans.*, 2019, **48**(41), 15465–15469.
28 P. Gkolfi, D. Tsivaka, I. Tsougos, K. Vassiou, O. Malina, M. Polaskova, C. D. Polyzou, C. T. Chasapis and V. Tangoulis, *Dalton Trans.*, 2021, **50**(38), 13227–13231.
29 A. Regueiro, M. Marti-Carrascosa, R. Torres-Cavanillas and E. Coronado, *Dalton Trans.*, 2024, **53**, 8764–8771.
30 T. Uemura and S. Kitagawa, *J. Am. Chem. Soc.*, 2003, **125**(26), 7814–7815.
31 V. Martínez, I. Boldog, A. B. Gaspar, V. Ksenofontov, A. Bhattacharjee, P. Gütlich and J. A. Real, *Chem. Mater.*, 2010, **22**(14), 4271–4281.
32 Y. Kobayashi, K. Misawa, M. Kobayashi, M. Takeda, M. Konno, M. Satake, Y. Kawazoe, N. Ohuchi and A. Kasuya, *Colloids Surf., A*, 2004, **242**(1–3), 47–52.
33 L. J. Ramírez-Cando, U. De Simone and T. Coccini, *J. Nanosci. Nanotechnol.*, 2017, **17**(1), 203–211.
34 J. Chomoucka, J. Drbohlavova, D. Huska, V. Adam, R. Kizek and J. Hubalek, *Pharm. Res.*, 2010, **62**(2), 144–149.
35 L. S. Arias, J. P. Pessan, A. P. M. Vieira, T. M. T. de Lima, A. C. B. Delbem and D. R. Monteiro, *Antibiotics*, 2018, **7**(2), 46.
36 Y. Chen, J. G. Ma, J. J. Zhang, W. Shi, P. Cheng, D. Z. Liao and S. P. Yan, *Chem. Commun.*, 2010, **46**, 5073–5075.
37 I. A. Gural'skiy, C. M. Quintero, G. Molnár, I. O. Fritsky, L. Salmon and A. Bousseksou, *Chem. – Eur. J.*, 2012, **18**, 9946–9954.
38 S. Sarkar, E. Guibal, F. Quignard and A. K. SenGupta, *J. Nanopart. Res.*, 2012, **14**(2), 715.
39 T. Castel, A. Marchetti, F. Houard, N. Daro, M. Marchivie, G. Chastanet and K. Bernot, *Cryst. Growth Des.*, 2023, **23**, 1076–1083.
40 S. A. Barrett, C. A. Kilner and M. A. Halcrow, *Dalton Trans.*, 2011, **40**, 12021–12024.
41 V. N. Ikorskii, *Dokl. Phys. Chem.*, 2001, **377**, 77–79.